Single Wake Meandering, Advection and Expansion - An analysis using an adapted Pulsed Lidar and CFD LES-ACL simulations

Machefaux, Ewan; Larsen, Gunner Chr.; Troldborg, Niels; Rettenmeier, Andreas

Published in:
Prodeedings of EWEA 2013

Publication date:
2013

Document Version
Publisher's PDF, also known as Version of record

Single Wake Meandering, Advection and Expansion - An analysis using an adapted Pulsed Lidar and CFD LES-ACL simulations

Ewan Machefaux †, Gunner C. Larsen †
Niels Troldborg † and Andreas Rettenmeier ‡

† Technical University of Denmark, Risø Campus, Department of Wind Energy
Building VEA-118, P.O box 49, DK-4000 Roskilde, Denmark
email: ewma@dtu.dk

‡ Stuttgart Wind Energy (SWE), University of Stuttgart
Allmandring 5B, 70569 Stuttgart, Germany

Correspondence: ewma@dtu.dk; 0045 21517545.

Abstract:

In this paper, single wake characteristics have been studied both experimentally and numerically. Firstly, the wake is studied experimentally using full-scale measurements from an adapted focused pulsed lidar system, which potentially gives more insight into the wake dynamics as compared to classical studies based on meteorological (met) masts and continuous wave lidar measurements, due to its capability of scanning several cross sections simultaneously. A wake center tracking procedure is used to estimate the sideways wake center displacements, also referred to as lateral meandering of the wake, and it is compared to the predictions from the Dynamic Wake Meandering model, for a selected 10 minutes dataset. Secondly, the average wake expansion in the fixed frame of reference is determined from measurements and compared to results from CFD simulations. The CFD simulations were conducted using the EllipSys3D flow solver using Large Eddy Simulation (LES) and Actuator Line Technique (ACL) to model the rotor. Discrepancies due to the uncertainties on the wake advection velocity are observed and discussed.

Keywords: Dynamic Wake Meandering; wake expansion; wake advection; pulsed lidar; CFD; Large Eddy Simulation; Actuator Line Method

1 Introduction

This paper is about validation of simple wake engineering models and CFD models using full-scale experimental data obtained from a pulsed lidar system. These validations are facilitated by the recent breakthrough in remote sensing technologies, their increasing reliability and the ease of installation in remote locations such as wind turbine nacelles. Specifically, three main aspects of the wake dynamics are studied in the present work: 1) the wake expansion in the meandering frame of reference, which corresponds to the increase in radial extend of the wake deficit caused by small scale turbulent diffusion and pressure recovery, as it convects downstream; 2) the advection velocity, which is the speed of the downstream transportation of the wake; and 3) the wake meandering, which relates to the continuous change of the lateral and longitudinal position of the wake deficit caused by the large turbulent structures of the atmosphere.

A previous study by Frandsen [1] showed, that wakes have a large impact on the aerodynamic behavior and lifetime of turbines within a wind farm. Therefore, good confidence in wake engineering models is required, so that they can be used extensively to assess and improve the performance of a wind farm layout or a rotor as well as wind farm control strategy.

A measurement campaign, resulting in full-scale wake lidar measurements, was conducted during the spring of 2011 at the DTU Wind Energy Risø campus test site. It involved a WindCube pulsed lidar system with a scanner device developed and adapted by the University of Stuttgart (SWE) to facilitate 2D lidar scan features. The lidar was mounted on the back of the nacelle of a stall regulated 500kW Nordtank wind turbine enabling scanning of the wake flow field simultaneously at different downstream cross sections. As opposed to the study in [2] based on continuous wave lidar technology, where the full-scale wake measurements are obtained in one particular downwind cross section only, a pulsed lidar offers

measurement of the wake expansion simultaneously in a specified number of downstream cross sections.

The meandering path of the wake can be extracted by identifying the wake center for each lidar sweep in all cross sections. It is consequently possible to compare prediction of wake meandering obtained from the Dynamic Wake Meandering model (DMW) [3] with the measured wake meandering in the specified cross sections. Such comparisons are of relevance for model calibration and validation, and provide more insight into the downwind convection of the wake.

Finally, CFD simulations are conducted with atmospheric characteristics and turbine operational conditions identical to a selected 10min time series from the campaign. The simulations are conducted using the Large Eddy Simulation approach for modeling the large atmospheric turbulence scales combined with the Actuator Line technique (ACL) to model the rotor. CFD results on average wake expansion in the fixed frame of reference are compared with measurements as well as predictions obtained from simple engineering models.

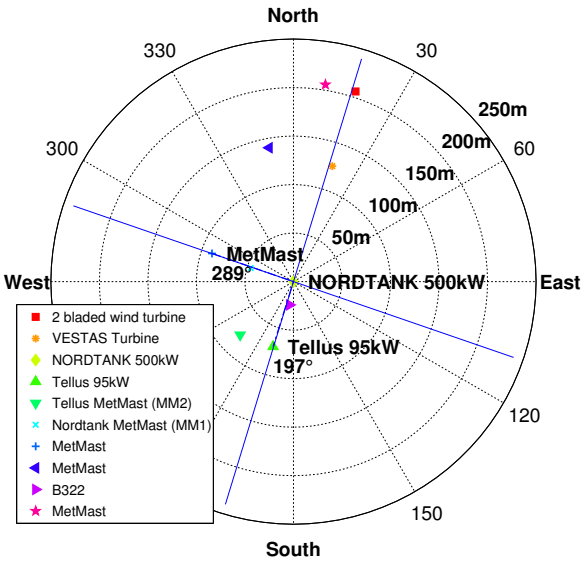

Figure 1: Risø test site descriptions, centered around the stall regulated Nordtank 500kW turbine, with a lidar mounted. Concentric circle indicates distance in meter from the Nordtank turbine. The location of a nearby turbine and obstacle have been determined by GPS during a previous campaign. The blue line $289\,^\circ$ represent the mean flow direction of the present study.

2 Experimental approach

2.1 The test set up

The DTU Wind Energy Risø campus test site consists of several turbines and meteorological masts on a nearly uniform and flat land nearby Roskilde Fjord, Denmark. Fig. 1 is a sketch of the test site with a description of turbines and met mast with their relative spacing. The present analysis focuses on single wake measurements behind the stall regulated Nordtank 500kW turbine for incoming winds with an inflow direction of $289\,^\circ$, where the met mast can provide undisturbed inflow measurements to the turbine.

The measurement set up involves a standard pulsed lidar system, Windcube WLS 7, where the scanner device has been adapted. Details on the adaptation and testing can be found in [4]. The raw lidar spectra are post processed by a software developed at SWE and stored in a database at DTU - Risø Campus, together with the data from the met mast and turbine operational sensors. The line-of-sight velocity vectors provided by the lidar system are projected on the main flow direction using the method described in [2]. Time synchronization between lidar and turbine related sensors is performed by the developed post processing software. A robust filtering procedure is implemented, in order to identify erroneous measurements resulting from ground reflection or nearby obstacles. This filtering basically relies on the plausibility of the measured wind speed and the Carrier to Noise Ratio (CNR) value of the laser beam. During the campaign, two distinct half-opening angle were used. The narrower scanning pattern corresponds to a half-opening angle of approximately $8.5\,^\circ$, and the wider one has a half-opening angle of $16.7\,^\circ$. A Cartesian scanning pattern, consisting of a set of 49 measurement target points each spanning 5 planes located at approximately 1,2,3,4 and 5 rotor diameters downstream is used, as depicted in Fig. 6. An example of the 10 min average line-of-sight velocities across the 5 scanning planes is shown on Fig. 3. The duration of a single sweep scanning, consisting of 49 measurements over each of the 5 planes, is approximately $7.8s$.

2.2 Resolving of the wake

In this section, the methods used to resolve the wake are detailed. The wake is resolved in two frames of reference: 1) the nacelle frame of reference (also referred as fixed frame of reference if we assume no yawing activity of the nacelle); and 2) the meandering frame of reference following the displacement of the wake. In order to determine the unsteady wake in the nacelle frame of reference, i.e. a set of 2D wake profiles corresponding to successive lidar sweeps, a “short term” wake averaging procedure is implemented similarly to that described in [2]. Each lidar sweep volume measurement are assigned into a so-

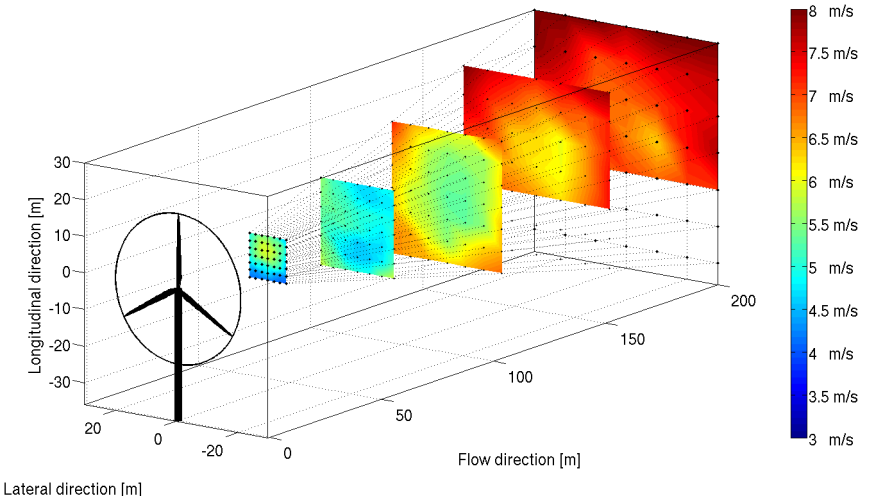

Figure 3: Projected view of a 10 minutes average wake flow field scanned by the pulsed lidar in the fixed frame of reference. The black dots are representing cartesian measurement points in the domain. The lower truncation of the 2 most downwind planes is the consequence of ground or obstacles detection. The coordinate system used in this study is right handed with x-axis along the main flow direction, the y-axis directed in the lateral direction, and z-axis vertical and pointing upwards.

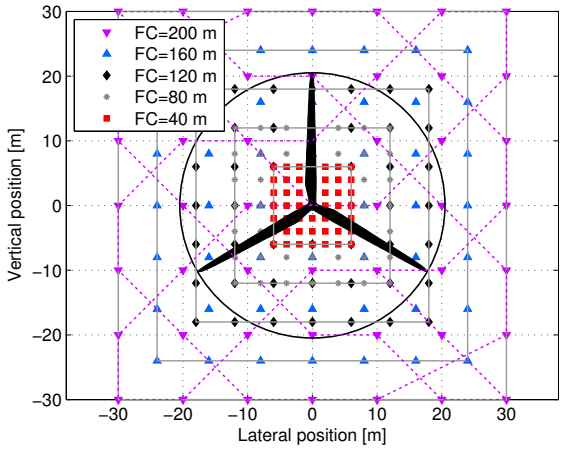

Figure 2: Superimposed grid based on the five lidar focus distances with a half-opening angle of $8.5\,^{\circ}$. The color points represent measurement locations at different downstream position. The beam trajectory is represented in dash lines for the plane at 200m downstream ($\approx 5D$, D corresponding to the rotor diameter).

called “wake slice”, with release time corresponding to the time average of all measurements within that particular sweep. Thus, “trains” of wake releases are resolved for each focus distance. Each wake slice are re-interpolated over a finer grid in order to handle the changes in grid spacing for each focus plane. The grid spacing of this global refined grid is equal to $1m$, corresponding to half of the grid spacing of the Cartesian scan pattern, at focus distance $40m$. A sketch of this averaging procedure is shown in Fig. 4.

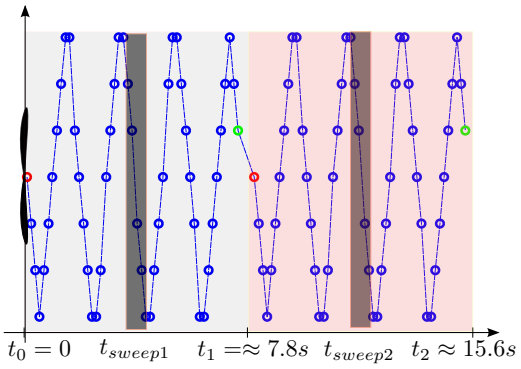

Figure 4: Sketch of the sweep averaging procedure seen from the side of the rotor. 2 Lidar sweeps are shown, one in blue and one in red. The 49 measurements points per sweep are shown in blue dots together with the measurement path as function of time. All measurements within one sweep are associated with a “2D wake slice” (dark), where its release time is defined by t_{sweep}, the time average for the relevant sweep.

The wake deficit is computed for each slice as based on the wake flow field, where the shear contribution is preliminary removed. Two methods are tested for the computation of the sheared inflow. The first one is based on the three sonic anemometer wind speed recorded at the met mast and uses a

power law fitting to obtain a mean inflow profile. The second method is to use directly the lidar measurements at the boundaries of the most downwind scanning planes to get an estimate of the shear profile. This latter approach is only used with time series, where the large half opening angle is used, in order to avoid any wake effect on the vertical wind profile. Furthermore, an averaging over a small vertical band of a few meters in horizontal extension is required to reduce the random scatter in the wind profile. Once the shear profile is known, the shear compensated flow is interpolated on the same global grid, in order to facilitate computation of the instantaneous wake deficit. An example, showing the comparison between the shear profile computed from each of the two methods, is shown in Fig. 5. It is seen that qualitatively the wind speeds are in fair agreement between the two methods when comparing with the lidar measurements at the two most downwind planes. However, a nearly constant offset along the vertical span in the order of $0.2 - 0.3m/s$ is observed, and the same trend is seen in other investigated dataset. The cause of this mismatch is currently being investigated. It is speculated that the combination of terrain orographic and roughness shift effects at the test site and from westerly winds affects the shear profile downwind, as measured by the lidar. This has to be taken into account in the subsequent wake expansion determination, since it will influence the choice of a suitable free wind speed. In the subsequent analysis, the use of the lidar for determining the shear is adopted. The fair shear gradient agreement seen in Fig. 5 gives a good confidence in using this method.

The transformation from the nacelle to the meandering frame of reference is performed by identifying the wake center for each wake slice, and subsequently transform the instantaneous flow field recordings to a Cartesian meandering frame of reference with origin at the wake center. The instantaneous wake center is obtained using an optimization based method similar to the one described in [5].

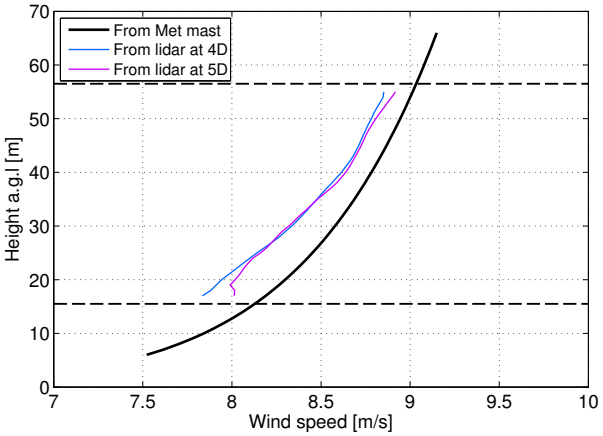

Figure 5: Comparison of the shear profile extracted from the met mast and using a power law fit (blue) with the profile measured by the lidar for two downstream cross sections. This profile is averaged over a 3m width band in both the left and the right boundaries of the scanning window. The horizontal dash lines represent the lower and upper part of the rotor.

3 Numerical approach

3.1 The flow solver and computational domain

The computation of the wake flow field has been carried out using the 3-D flow solver EllipSys3D developed by Michelsen and Sørensen [6], [7]. It solves the discretized incompressible Navier-Stokes equations in general curvilinear coordinates using a block-structured finite volume approach. EllipSys3D is formulated in primitive variables (pressure-velocity) in a non-staggered grid arrangement. The pressure correction equation is solved using the SIMPLE algorithm, and pressure decoupling is avoided using the Rhie/Chow interpolation technique. The convective terms are discretized using a hybrid scheme combining the third-order accurate Quadratic Upwind Interpolation for Convective Kinematics (QUICK) scheme (90%) and the fourth order Central Difference (CDS) Scheme (10%). The Large Eddy Simulation approach (LES) is adopted, employing the mixed subgrid scale (SGS) model described in [8]. The used mixed SGS viscosity model depends on a filter function and empirically determined constants chosen according to previous work on wake simulations [9].

The wind turbine rotor is simulated using the actuator line model (ACL) developed in [10]. This model combines a three-dimensional (3-D) solver with a technique, in which body forces are distributed radially along lines representing the blades of the wind turbine and smeared azimuthally using a suitable Gaussian smearing function. The standard deviation of the Gaussian function is taken as $3\Delta_x$, where Δ_x is the local grid spacing at the rotor, as based on recommendations from a previous numerical wake study [11]. The body forces are obtained by a look-up table of airfoil data where the local angle of attack is used. In the present study, the blade is discretized using 31 point per radius in the ACL model.

Assuming a homogeneous turbulent field, the modeling of the atmospheric boundary layer (ABL) is done based on the average turbulent intensity and the shear profile as extracted from the measurements. Similarly to [9], the sheared atmospheric

mean velocity field is imposed at the inlet of the domain. Additionally, the turbulence field, represented by all three turbulence components of a 3-D incompressible flow field is generated prior to the computation using the Mann algorithm [12], which reproduces homogeneous, stationary, Gaussian and anisotropic turbulence with the same spectral characteristics as observed in the neutrally stratified atmosphere. The Mann spectral tensor is developed using rapid distortion theory combined with a model for eddy lifetime as well as with assumptions of linear shear and neutral stratification. The dimensions of the generated turbulence box is approximately $(Lx, Ly, Lz) = (18R, 18R, 300R)$, where R is the rotor radius, and the number of grid points in the box is $128X128X2048$, resulting in a grid with a resolution corresponding to 7 grid points per rotor radii. The turbulence is introduced in a cross section plane 1.5D upstream of the rotor.

The computational domain has 17.92 million grid points. The dimensions of the grid used (Lx, Ly, Lz), expressed in terms of rotor radius R, are respectively $(28R, 28R, 36R)$. The grid layout and the boundary conditions are in accordance with previous studies on wake computation [9] and [2]. The inlet of the domain is applied with the desired average wind shear profile as measured at the test site; the outlet has unsteady convective conditions; the ground of the domain has a wall no slip condition; and the top boundary is set to the farfield velocity. The cells are concentrated with a constant spacing of $\Delta_x = \frac{R}{30}$ in the finest resolved wake region in order to resolve and preserve the wake structures. Upstream of the location, where turbulence is introduced, a coarser equidistant region with a spacing $\Delta_x c = \frac{R}{15}$ is used. Finally, stretched regions extend to the inlet and outlet of the domain, respectively. A layout of the computational domain is shown in Fig. 6.

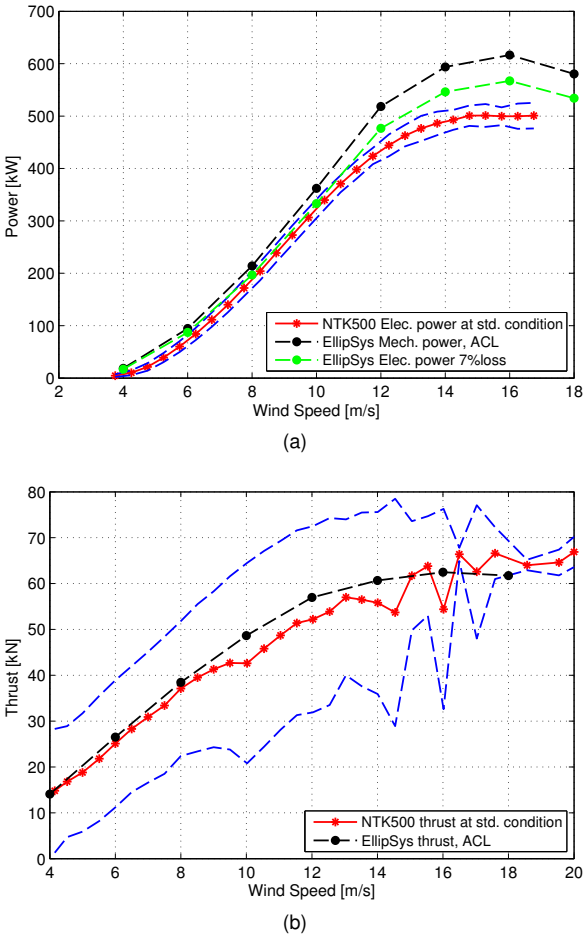

Figure 7: Comparison between measured power and thrust curve at standard conditions (TI $< 10\%$, 15^oC and 1013.3mbar) with simulations. UPPER: Power curve of stall regulated 500kW Nordtank turbine. The overshoot seen in the simulation at high wind speed is due to the stall not being modeled. LOWER: thrust curve derived from two tower bottom bending moment signals. The blue dash lines represent $\pm\sigma_P$ and $\pm\sigma_T$, the standard deviation of the power and the thrust, respectively.

3.2 Validation of the numerical model

In this section, a validation of the numerical model is performed. First of all, the ACL model implementation is validated by comparing the measured power curve and thrust curve (derived from two tower bottom bending moment signals) of the Nordtank 500kW with results from the simulations. The measured power curve is determined according to the IEC-61400 standard. The electrical power produced is obtained assuming 7% loss from the available rotor mechanical power, according to [13]. Results of the comparison are shown in Fig. 7.

From Fig. 7, it is seen that the CFD simulations are able to predict fairly well the electrical power produced up to $12m/s$. Above that wind speed, the rated wind speed of the stall regulated turbine is reached, and the separation occurring in the stall region is not properly captured by the model. This, however, has no impact on the subsequent study, since time series with 10 minutes average wind speeds of up to $8.5m/s$ are used in the analysis. Equally good agreement is seen with the thrust comparison.

Secondly, single wake deficit resolved in the meandering frame of reference are compared to measurements for the five available cross sections. The determination of the wake deficit in the meandering frame of reference for the nearest cross section ($1D$ downstream) is not reliable due to the restricted amount of time, where the wake center is located within the

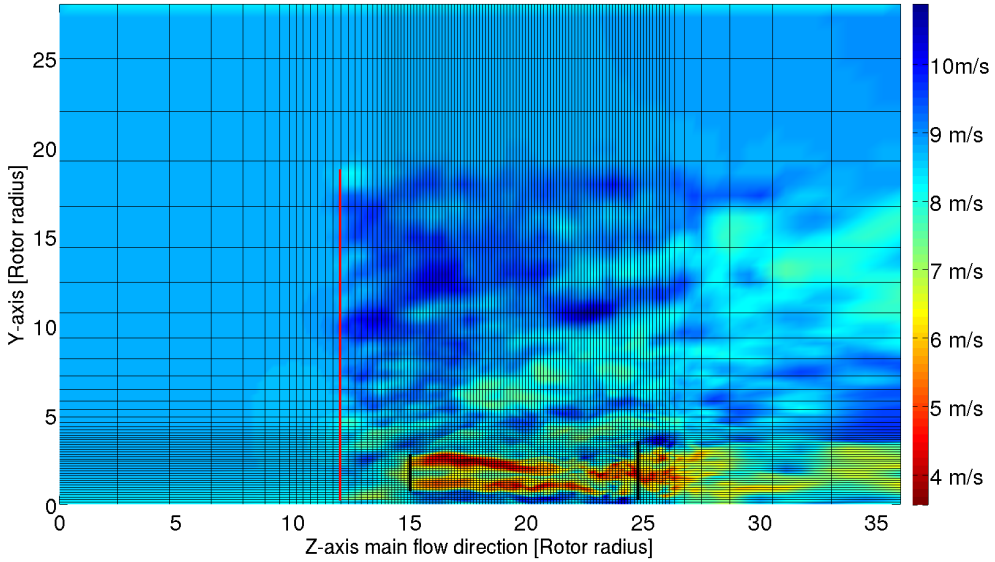

Figure 6: Overview of the computational domain. Every 4th cell face is represented. The average streamwise, velocity extracted from a cross section in the middle of the domain ($L_x = 14R$), is shown in a background contour plot. The red line indicates the location of introduced turbulence generated using the Mann model prior to the computations. The locations of the Nordtank turbine is shown in the black line at $L_z = 15R$. The most downwind lidar cross section is shown in black line at $L_z = 24.75R$.

scanning area. Results of the comparison are presented in Fig. 8.

From Fig. 8, discrepancies are observed between the measured and the simulated wake deficit around the wake center, 1D and 2D downstream, respectively. The measured wake deficit at $2D$ is not symmetric and is slightly distorded. This is due to the difficulties for the tracking procedure to identify the wake center for the entire 10 minutes time span. The discrepancies at the wake center tends to disappear with increasing downstream distance, where the reliability of the tracking procedure increases due to the increase of the lidar scanning area in lateral direction. The overall agreement between measurement and simulation is good.

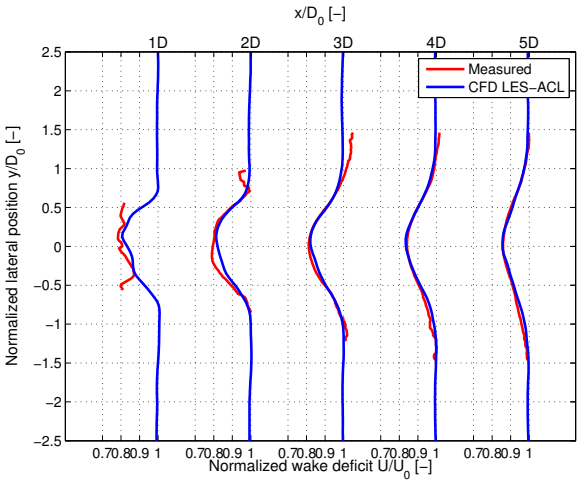

Figure 8: Normalized wake deficit at hub height in the meandering frame of reference for all five available downstream cross sections. The top x-axis represents the downstream position in rotor diameters. The bottom x-axis show the normalized wake deficit. The y-axis represents the normalized lateral position. D_0 denotes the rotor diameter and U_0, the average free stream velocity.

4 Results and discussion

4.1 Single wake meandering dynamics

4.1.1 DWM model implementation

The main conjecture behind the Dynamic Wake Meandering model (DWM) [3] is that the transport of wakes in the atmospheric boundary layer (ABL) can be modeled, by considering the wakes to act as passive tracers driven by the large-scale turbulence structures. In the present study, the DWM model is implemented similarly to [5], where the modeling of the wake meandering relies on a suitable description of the large-scale turbulence structures of the atmospheric boundary layer, as well as of a suitable definition of cut-off frequency.

On one hand, the wake dynamics along the main

flow direction is modeled using Taylor's frozen turbulence hypothesis. The downstream advection of the "emitted" wake deficits is assumed to be driven by the constant Taylor advection velocity U_T, which in the present work is computed as the reduced wind speed behind a turbine as initially proposed in the N.O. Jensen's model [14] and summarized in [15]. This simplification decouples the wake along wind deficit profile (and expansion) and the downstream transportation process.

On the other hand, the wake dynamics in the lateral and vertical directions is modeled by considering a cascade of wake elements (also referred previously to as "wake slices") displaced according to the large-scale lateral and vertical turbulence velocities at the position of the particular wake cascade element at each time instant. The transverse velocity field $(v_c(t), w_c(t))$, associated with the large scale part of the turbulence field, recorded by means of 3 sonics anemometers located upstream of the rotor (at $89m$, $\approx 2.2D$), with the mean wind direction aligned towards the rotor, and where large scale filtering is applied using a cut-off frequency corresponding to a spatial scale of two rotor diameter, as based on previous recommendations by Larsen et. al. [3].

In order to compute a wake displacement at a specific position and time, time synchronization of the various signals is required. Specifically, the signal time lag t_0 caused by the spatial separation between the met tower (sonic signals) and the turbine (thrust derived signals, yaw signals) is determined as specified in Eq. (1), whereas a second time lag $t_w(FC)$, representing the time an air particle uses to travel from the rotor to the downstream position FC, is estimated as in Eq. (2). Consequently, the total transportation time $t(FC)$ for an air particle to move from the sonic anemometers location to a lidar scanning plane is the sum of both time lags $t_w(FC)$ and t_0 (Eq. (3)).

$$t_0 = \frac{D_{mr}}{U_0} \tag{1}$$

$$t_w(FC) = \frac{FC}{U_{adv}} \tag{2}$$

$$t(FC) = t_0 + t_w(FC) \tag{3}$$

where D_{mr} is the distance between the mast and the rotor ($\approx 89m$), U_0 is the average free stream velocity, FC is the lidar focus distance, in this case (40,80,120,160 and 200m), respectively, and U_{adv} is the advection velocity computed according to N.O Jensen's model.

In order to compute the wake displacement at a given downstream position (FC) and at a given time, the transverse large scale transverse turbulence velocities (v_c,w_c), the wind directions obtained from the sonic anemometers and the turbine related sensors are expressed in a common time frame $\tilde{t}(FC)$. This common time frame ensure that all sensors are synchronized with respect to the 5 downstream position, and that the relevant time delay is applied to each signal. A sketch representing signal time lines and their corresponding delay is shown on Fig. 9.

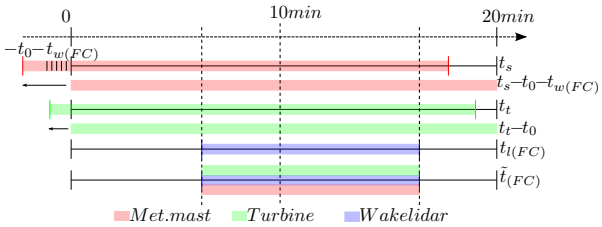

Figure 9: Timeline of various measurements. 20 min met mast and turbine measurements are used to cover a 10 minute lidar measurement time series with random start and stop time.

Thus, following the DWM hypothesis, the lateral and vertical wake meandering dynamics (wake displacements) are determined for all downstream cross sections as:

$$y(FC, \tilde{t}) = v_c(\tilde{t}) \cdot \tilde{t}(FC) + h_{yaw}(FC, \tilde{t}) \tag{4}$$
$$z(FC, \tilde{t}) = w_c(\tilde{t}) \cdot \tilde{t}(FC) + h_{tilt}(FC, \tilde{t})$$

The tilt contribution $h_{tilt}(FC, \tilde{t})$ is disregarded in the present study since the lidar scanning head was aligned horizontally with the ground and not with the nacelle titled by 2^o. Thus, only the sideways meandering motion of the wake is investigated. The contribution of the turbine yaw misalignment $h_{yaw}(FC, \tilde{t})$ to the wake displacement is taken into account as:

$$h_{yaw}(FC, \tilde{t}) = FC \cdot \tan\left(\theta_s - \theta_{yaw}(\tilde{t}(FC))\right) \tag{5}$$

where the misalignment angle is computed from the measurement of yaw position of the turbine $\theta_{yaw}(\tilde{t}(FC))$ and the mean wind direction from the met. mast sonic sensors (average of 3 available heights) θ_s, as detailed in Fig. 10.

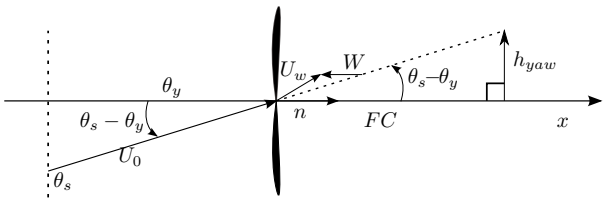

Figure 10: Sketch of the wake displacement due to yaw misalignment. The rotor orientation angle θ_y is the reference and is obtained from the absolute yaw position sensor. The misalignment angle is the difference between the wind direction (θ_s) and the absolute rotor position.

4.1.2 *Comparison of measured meandering with results from DWM*

A dataset was selected with the inflow direction aligned along the line connecting the turbine and met mast, a low yawing activity throughout the 10 minutes and a mean free stream velocity of $8.1m/s$. Furthermore, the mean turbulence intensity, defined as the ratio between the standard deviation and the mean of the wind speed, is 11% and the shear exponent obtained from power law fitting of the free wind profile is 0.1. With input from the met mast, the DWM model is used to predict the wake center displacements as function of time using the implementation described in the previous section, whereas the result from the tracking algorithm gives an estimate of the wake center displacements from the lidar measurements. Both results are compared in Fig. 11 for a downstream distance of 3 rotor diameters.

The agreement between measured (blue curve) and modeled meandering (magenta curve) is reasonable, however; an offset or "time lag" is seen which is most pronounced between 100s and 140s. In this time interval, the tracking procedure doesn't perform properly due to the restriction of finding the wake center within the measurement area. It seems that the wake meandering is too large, so that the wake center is outside the lidar scanning area, however, the model is able to predict such large meandering of the wake. The time lag indicates that, in the context of DWM modeling, the use of the reduced wind speed behind a rotor according to the N.O. Jensen's model is not representative for the wake advection velocity, however, the overall fair agreement confirms that it is a good initial guess. Furthermore, the offset can be the consequence of using a constant advection velocity over the considered time span where large scale velocity trends in the mean wind direction is not accounted for. As good agreement can be observed for a given period within a 10 minutes time series, whereas larger deviation can occur elsewhere. This seem to be the most plausible explanation of the local deviation seen in the present comparison.

In order to quantify the time offset, and thus get an estimate of the mean advection time difference, a cross correlation study is performed between measured (W_m) and simulated time series (W_s). The DWM time series is slided in time τ (where τ is approximately ranging as $-600s < \tau < 600s$) relative to the tracked time series, and the cross correlation coefficient is computed for each τ. The time offset τ, that yields the maximum cross correlation coefficient, is the sought time offset.

$$\rho(\tau) = \frac{R(\tau)}{\sigma_{W_s}\sigma_{W_m}} = \frac{E\left[(W_s(t+\tau) - <W_s>)(W_m(t) - <W_m>)\right]}{\sigma_{W_s}\sigma_{W_m}} \quad (6)$$

where E is the expected value operator, t is the time, σ_W is the standard deviation of the displacement, and $< W >$ refers to the average of the wake center displacement in time. In practice, a cross correlation algorithm doesn't change the characteristics of the time series, as it slides one relative to the other, however, it the context of the DWM, the change in transportation time affect the amplitude of the meandering as seen from Eq. (4) and depicted in Fig. 11. It is seen, that the amplitude of displacement of the green curves is increasing when increasing the transportation time (which in turn decreases the advection velocity since a longer time is required to reach a particular downstream position). The blue curve represent calibrated DWM result yielding the highest cross correlation. The corresponding mean transportation time lag is in the order of $5.5s$, which is smaller than the sweep averaging time. Results of the analysis are summarized in the following Table 1, where the raw DWM results are shown together with the modified advection time and advection velocity obtained from the cross correlation calibration.

Table 1: Advection velocities and transportation time at 3D downstream and from the two estimation methods. $U_0 = 8.1$m/s and $t_0 = 11s$. U_w from the N.O Jensen model is computed as: $U_w = \sqrt{1 - CT} \cdot U_0$.

	U_w	t	t_{adv}
DMW Raw	3.4m/s (N.O. Jensen)	46s	35s
DMW Calibrated	4.06m/s	40.5s	29.5s

To conclude, the mean advection velocity of a wake "slice" during its convection from the rotor location to 3D diameters downstream is, in the present case, underestimated by using N.O Jensen model formulation.

4.2 Single wake expansion

In this section, the wake expansion in the fixed frame of reference is computed from a selected dataset representing high rotor thrust coefficient and well resolved wake in all 5 downstream cross sections. The selected dataset has a similar inflow and operational conditions to the previous dataset, i.e., an average free stream velocity of $8.6m/s$, a shear exponent of 0.08 and a turbulence intensity of 13.5%. The large lateral half opening angle of the scanner head of $16.7\,^\circ$ is used. By operating the lidar at a large opening angle, it is ensured that the full extent of the wake

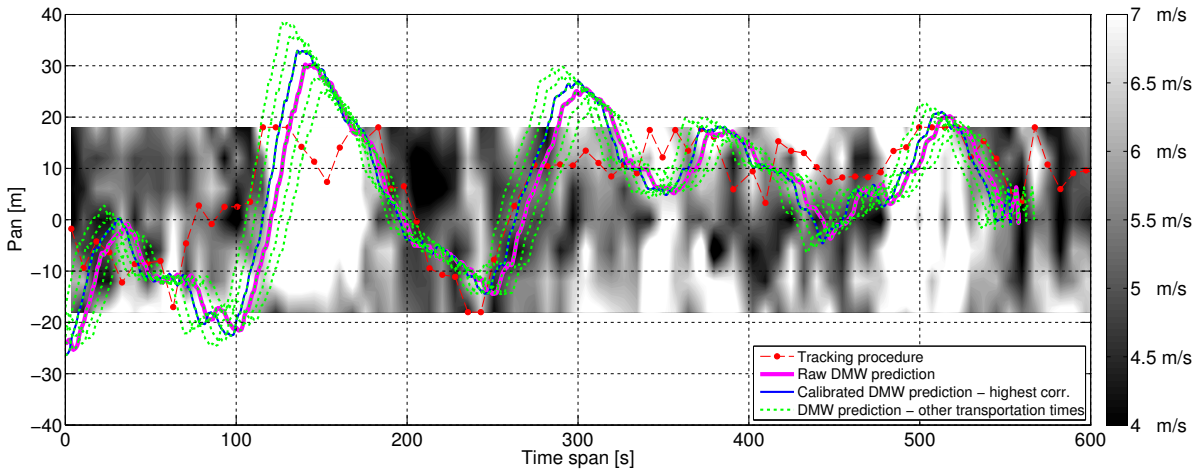

Figure 11: Lateral wake meandering analysis at FC=120m ($\approx 3D$). The tracked wake deficit center (using similar technique as in [5]) is shown in red dotted line. The prediction from the DWM model, obtained using the spatially averaged inflow velocity of three sonic anemometers minus the measured nacelle displacement (yaw contribution), is shown in magenta. The background gray density plot represents the measured wake at hub height. Low wind speed is shown in black, and higher wind speed is shown in white. The green dashed lines represent several transportation time lags τ from the cross correlation study. The blue line is the model prediction leading to the highest cross correlation with the tracked wake.

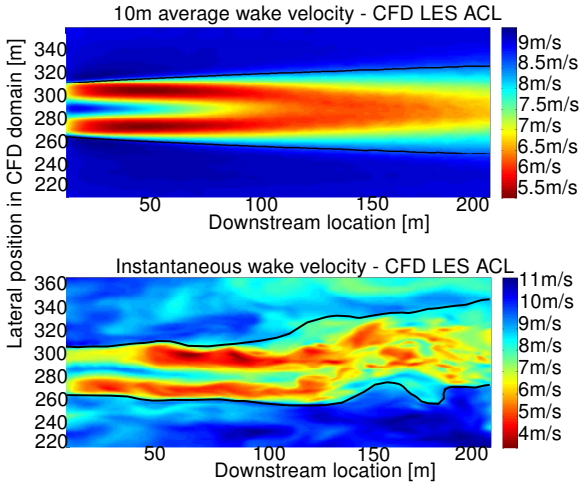

Figure 12: Wake velocity field extracted from a slice of the computational domain at hub height and wake width determination from CFD LES ACL. TOP: 10 minute average wake velocity, and BOTTOM: quasi-instantaneous wake velocity. Wake boundaries are shown in black line.

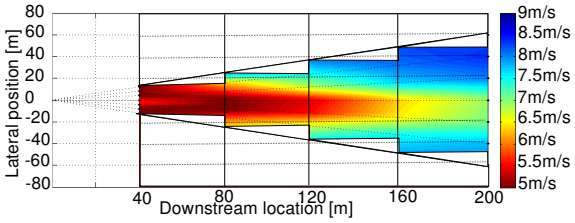

Figure 13: Example of wake velocity field extracted from the lidar measurement at hub height and seen from above. 2-D interpolation between the cross sections is performed to obtain the average flow field in the entire measurement region.

meandering is captured for the expansion study. Typically, the 10 minute average wake width is computed as the extend defined by the lateral coordinates of the intersection between the average wake deficit at hub height and the mean free stream velocity. In practice, the choice of a suitable free stream velocity, giving a realistic wake expansion, is rather challenging. In fact, as discussed previously in the experimental approach section, the observation of several time series show that the measured free stream velocity at the met mast is often higher than the free stream velocity measured by the lidar around the wake, as depicted on Fig. 5.

Results for the wake expansion coefficient, as defined by the ratio of the wake width, at a given downstream position, and the rotor diameter D_0, are compared to the modified wake expansion model of Frandsen in Rathmann et. al. [15], the Theodorsen

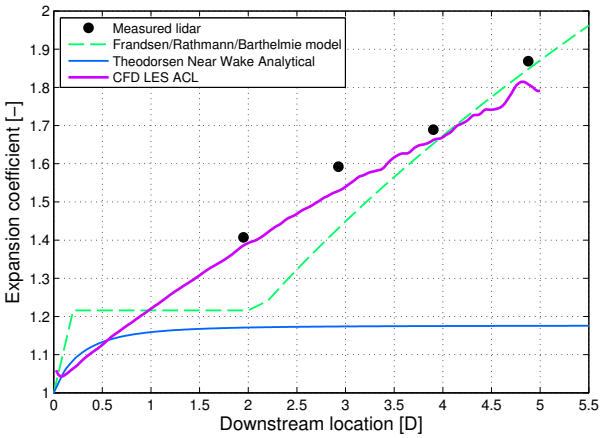

Figure 14: Comparison of 10 minutes measured average wake expansion including pressure recovery with a modified Frandsen engineering mode, Theodorsen's near wake analytical solution; and CFD ACL LES simulation. Black dots are measurements.

Near Wake Analytical solution derived in [16] and implemented in [17], and the present CFD ACL LES unsteady simulation similar to [9] and [2]. The average wake expansion is determined from CFD by computing the wake width from the average streamwise velocity at hub height, as depicted in Fig. 12(a). The 10min average streamwise velocity field is obtained in the fixed frame of reference by averaging all instantaneous velocity field (Fig. 12(b)), extracted during the computation with a time resolution of 2sec.

The comparison presented on Fig. 14 shows good agreement between the measured and the CFD simulated average expansion. Furthermore, Theordorsen's analytical near wake model seems to predict fairly well the near wake expansion, when compared to the results from CFD LES ACL. Larger deviation are seen in the use of the modified Frandsen engineering model for downstream position up to 3 diameters. The agreement becomes more convincing in the far wake.

5 Conclusion

In the present study, single wake characteristics have been studied both experimentally and numerically. The measured wake meandering pattern is obtained from the tracking of the wake center and is compared with the predictions from the DWM model. Good agreement is observed despite of a phase lag due to the uncertainties in using the constant wake advection velocity as predicted in N.O Jensen model. A cross correlation study revealed a time offset of 5.5sec in average between the measured and modeled meandering paths.

The average wake expansion in the fixed frame of reference is determined from the available lidar cross sections and subsequently compared to simple engineering models as well as results from CFD simulations using LES and ACL. Good agreement is observed.

The present analysis is currently being extended to the development of a new wake expansion engineering model and an empirical relationship between the wake deficit magnitude and the advection velocity determined from the available meandering patterns. Moreover, selected consequencies of the DWM approach are currently being validated using this pulsed lidar measurement campaign.

6 Acknowledgments

This study has been founded by the DSF FlowCenter project (contract 2104-09-0026). The authors would like to acknowledge Kurt S. Hansen from DTU Wind Energy for providing measured thrust and power curves for the Nordtank 500 KW turbine. Furthermore, the authors would like to acknowledge the team of technicians from DTU Wind Energy TEM, for their work in the setting up of the lidar system as well as the data storage environment.

Bibliography

[1] S. T. Frandsen. Turbulence and turbulence generated structural loading in wind turbine clusters. *Risø-R-1188(EN), Risø National Laboratory, Roskilde, Denmark*, 2007.

[2] E. Machefaux, N. Troldborg, C. G. Larsen, J. Mann, and H. Aa. Madsen. Experimental and Numerical Analysis of Wake to Wake Interaction in Wind Farms. *EWEC 2012 Copenhagen. Scientific proceedings*, pages 100–104, 2012.

[3] G. C. Larsen, H. Aa. Madsen, K. Thomsen, and T. J. Larsen. Wake Meandering: A Pragmatic Approach. *Wind energy*, pages 11:377–395, 2008.

[4] A. Rettenmeier, O. Bischoff, M. Hofsäß, D. Schlipf, and J. J. Trujillo. Wind Field Analysis Using A Nacelle-Based Lidar System. *EWEC Warsaw 2010, Scientific Proceedings*, 2010.

[5] F. Bingöl, G. C. Larsen, and J. Mann. Lidar Measurements of Wake Dynamics, Part 1: One-dimensional scanning. *Wind energy 13, 51-61*, 2010.

[6] J. A. Michelsen. Block Structured Multigrid solution of 2D and 3D elliptic PDE's. Dept. of Fluid mechanics, DTU. *AFM 94-05*, 1994.

[7] N. N. Sørensen and W. Z. Shen. General purpose flow solver applied to flow over hills, PhD Thesis, Risø National Laboratory. *Wind energy*, 1995.

[8] L. Ta Phuoc, R. Lardat, M. Coutanceau, and G. Pineau. Recherche et analyse de modeles de turbulence de sous mailles adaptes aux ecoulements instationnaires decolles. limsi, france. *LIMSI Report 93074*, 2002.

[9] N. Troldborg, G. C. Larsen, H. Aa. Madsen, K. S. Hansen, J. N. Sørensen, and R. Mikkelsen. Numerical Simulations of Wake Interaction between Two Wind Turbines at Various Inflow Conditions. *Wind Energy, 14, doi: 10.1002/we.433*, pages 859–876, 2010.

[10] J. N. Sørensen and W. Z. Shen. Numerical modeling of Wind Turbine Wakes, Fluids Engineering, Vol 124, Issue 2. *Wind energy*, 2002.

[11] N. Troldborg. *Actuator Line Modeling of Wind Turbine Wakes, PhD Thesis*. 2008.

[12] J. Mann. The spatial structure of neutral atmospheric surface-layer turbulence. *Journal of fluid mechanics*, pages 273, 141–168, 1994.

[13] S.M. Petersen. Konceptundersøgelse Nordtank NTK 500/41, Måling af effektcurve. *Risø-I-799(DA)*, 1994.

[14] N. O. Jensen. A note on wind turbine interaction. *Risø-M-2411, Risø National Laboratory, Roskilde, Denmark*, 1983.

[15] O. Rathmann, R. Barthelmie, and S. Frandsen. Turbine Wake Model for Wind Resource Software. *EWEC 2006 Wind Energy Conference and Exhibition, Scientific Proceedings*, 2006.

[16] T. Theodorsen. Theory of propellers. *New York McGraw-Hill Book Company*, 1948.

[17] E. Branlard and M. Gaunaa. Development of new tip-loss corrections based on vortex theory and vortex methods. *The Science of Making Torque from Wind 2012, Oldenburg*, 2012.